Remote Sensing of Environment 113 (2009) 2037–2051

Contents lists available at ScienceDirect

Remote Sensing of Environment

journal homepage: www.elsevier.com/locate/rse

REVIEW

Remote sensing of solar-induced chlorophyll fluorescence: Review of methods and applications

M. Meroni [a,*], M. Rossini [a], L. Guanter [b], L. Alonso [c], U. Rascher [d], R. Colombo [a], J. Moreno [c]

[a] Remote Sensing of Environmental Dynamics Lab., DISAT, University of Milan-Bicocca, P.zza della Scienza 1, 20126, Milan, Italy
[b] GFZ German Research Centre for Geosciences, Telegrafenberg A17, 14473, Potsdam, Germany
[c] Image Processing Laboratory, LPI, University of Valencia, P.O. Box 22085, Valencia, Spain
[d] Institute of Chemistry and Dynamics of the Geosphere, ICG-3: Phytosphere, Forschungszentrum Jülich, Leo-Brandt-Str, 52425 Jülich, Germany

ARTICLE INFO

Article history:
Received 25 February 2009
Received in revised form 14 May 2009
Accepted 14 May 2009

Keywords:
Solar-induced chlorophyll fluorescence
Passive techniques
Methods
Applications
Devices

ABSTRACT

Interest in remote sensing (RS) of solar-induced chlorophyll fluorescence (*F*) by terrestrial vegetation is motivated by the link of *F* to photosynthetic efficiency which could be exploited for large scale monitoring of plant status and functioning. Today, passive RS of *F* is feasible with different prototypes and commercial ground-based, airborne, and even spaceborne instruments under certain conditions. This interest is generating an increasing number of research projects linking *F* and RS, such as the development of new *F* remote retrieval techniques, the understanding of the link between the *F* signal and vegetation physiology and the feasibility of a satellite mission specifically designed for *F* monitoring. This paper reviews the main issues to be addressed for estimating *F* from RS observations. Scattered information about *F* estimation exists in the literature. Here, more than 40 scientific papers dealing with *F* estimation are reviewed and major differences are found in approaches, instruments and experimental setups. Different approaches are grouped into major categories according to RS data requirements (i.e. radiance or reflectance, multispectral or hyperspectral) and techniques used to extract *F* from the remote signal. Theoretical assumptions, advantages and drawbacks of each method are outlined and provide perspectives for future research. Finally, applications of the measured *F* signal at the three scales of observation (ground, aircraft and satellite) are presented and discussed to provide the state of the art in *F* estimation.

Contents

* Corresponding author. Tel.: +39 02 64482848; fax: +39 02 64482895.
E-mail address: michele.meroni@unimib.it (M. Meroni).

0034-4257/$ – see front matter
doi:10.1016/j.rse.2009.05.003

1. Introduction

Monitoring plant status and function from space is of major interest for precision farming, forest management and assessment of the terrestrial carbon budget. Current strategies in optical remote sensing (RS) mainly rely on reflectance data offered by several Earth observing systems which provide estimates of plant status related to structural or biochemical properties such as leaf area index (LAI) or chlorophyll (Chl) content (e.g. Baret et al., 2007). These data can be used to model the potential photosynthetic rates of plant ecosystems. However, plant photosynthesis is an actively regulated process and the efficiency of this biophysical/biochemical reaction is highly variable, in that it adjusts to prevailing environmental conditions by altering or rearranging the pigments within the leaves without any detectable changes in reflectance.

An alternative to this strategy is offered by solar-induced Chl fluorescence (F) which is emitted by the photosynthetic machinery itself and which can provide an early and more direct approach for diagnosis of the actual functional status of vegetation, for example in detecting sub-optimal conditions before significant reductions in Chl content or LAI have occurred. In fact, the emission of light as F is in competition with photochemical conversion and therefore F may allow a more accurate carbon assimilation estimate and earlier stress detection than is possible from reflectance data alone (Entcheva Campbell et al., 2008).

Even though the first attempts to quantify F passively (i.e. without an artificial excitation source) on terrestrial vegetation date back to the 1970s, the challenging issue of the remote measurement of F is still in a developmental stage. Spaceborne observation of F was the concept defining the scientific Fluorescence Explorer (FLEX) satellite mission, submitted to the European Space Agency (ESA) Earth Explorer program call in 2005. Preparatory pre-phase A studies were performed from 2006 to 2008 (www.esa.int/esaLP/LPfuturemis.html, www.esa.int/esaLP/SEMQACHYX3F_LPfuturemis_0.html). Prompted by FLEX, research intensified greatly and resulted in a rapid improvement of F-sensing capabilities during this period. The aim of this manuscript is to provide a comprehensive review of the current methods and devices used to estimate F over terrestrial vegetation together with their applications at different observation scales, from ground to airborne and spaceborne measurements.

1.1. Origin of solar-induced Chl fluorescence

Chlorophyll fluorescence can be considered a direct probe of the functional status of photosynthetic machinery because of its relationship with photosynthesis. Typically, part of the energy absorbed by Chl is expelled from the light reactions of photosynthesis and is dissipated as fluorescence (re-emission of light at a longer wavelength than for excitation). Together with the other dissipative pathway, non-photochemical quenching (NPQ or non-photochemical protection), F competes with photosynthesis for the use of the absorbed light. This close relationship enabled plant physiologists to use field- or laboratory-based actively-induced fluorescence measurements as a diagnostic tool to assess the vitality of the photosynthetic apparatus (for a comprehensive overview see Papageorgiou & Govindjee, 2004, for a recent review see Baker, 2008).

Chlorophyll of the pigment–protein complexes exhibits a F emission spectrum in the red and near-infrared regions, characterized by two peaks at approximately 690 and 740 nm (Fig. 1A).

Although fluorescence, photosynthesis and non-photochemical protection are closely connected, the translation of fluorescence data to photosynthesis is not trivial. In fact, while under low light unstressed conditions (no non-photochemical protection mechanisms activated) a negative correlation exists between fluorescence and photochemistry, most studies have observed that in the presence of plant stress and high light conditions, fluorescence declines with photosynthesis (i.e., positive correlation) as a result of protective mechanisms (e.g., deactivation of the antenna, activation of the xanthophyll cycle and non-photochemical protection) which take place in the leaf to prevent damage caused by harmful radicals formed in such stress conditions (Van der Tol et al., 2009).

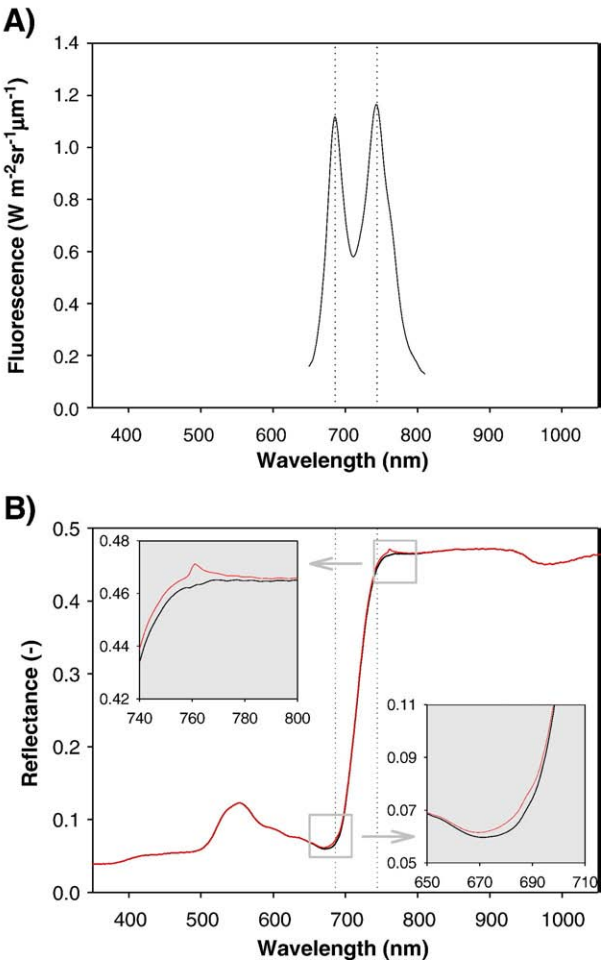

Fig. 1. Solar-induced Chl fluorescence and reflectance spectra of a sugar beet leaf. A): F spectrum in the region between 650 and 800 nm. B): The actual reflectance (black curve) was computed as the ratio of the reflected and incident fluxes; the apparent reflectance (red curve) was computed as the ratio of the total upwelling flux (reflection plus F) and the incident flux. The difference between the two quantities is highlighted in the grey boxes, showing the responses surrounding the F emission maxima (vertical dotted lines). Measurements were performed under solar illumination with an ASD FieldSpec FR Pro (FWHM = 3.5 nm) coupled with the FluoWAT leaf clip (Alonso et al., 2007b) which enables the extraction of the F spectrum by selectively filtering the incoming light (Zarco-Tejada et al., 2000a). FluoWAT employs a shortpass filter that blocks the incident light in the spectral range of F emission (wavelength>650 nm) so that the upwelling radiance in this region is purely composed of F. Data courtesy of C. Plückers. (For interpretation of the references to colour in this figure legend, the reader is referred to the web version of this article.)

1.2. F signal in remotely-sensed data

Plant fluorescence under solar illumination (F) adds a weak signal to reflected solar radiation. If both fluorescence emission and surface reflectance are assumed to follow Lambert's law, the radiance upwelling from vegetation (L) at ground level is therefore composed of two coupled contributions, one reflected ($r\,E/\pi$) and the other emitted (F):

$$L(\lambda) = \frac{r(\lambda)E(\lambda)}{\pi} + F(\lambda) \quad \left[\mathrm{W\,m^{-2}\,sr^{-1}\mu m^{-1}}\right] \tag{1}$$

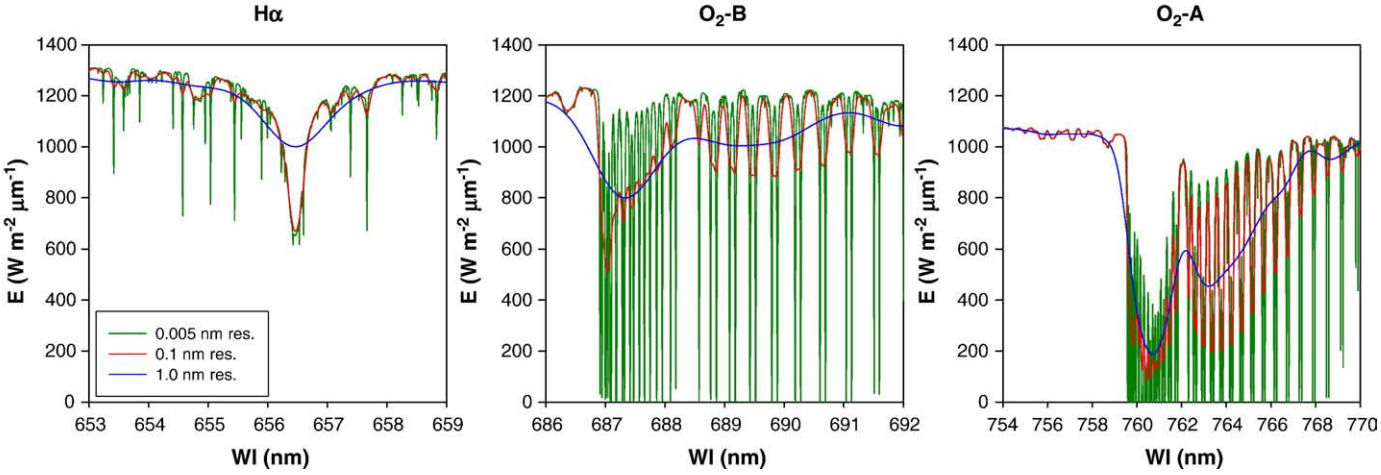

Fig. 2. Incident irradiance (E) at ground level at the three absorption lines normally used for F retrieval and at three different spectral resolutions (0.005, 0.1 and 1.0 nm for the green, red and blue curves, respectively). Data were simulated by the MOMO atmospheric radiative transfer code. The three lines are situated at 656.4 nm (Hα), 687.0 nm (O_2-B) and 760.4 nm (O_2-A). (For interpretation of the references to colour in this figure legend, the reader is referred to the web version of this article.)

where λ is wavelength, r is reflectance (free of the emission component), and E is total irradiance incident on the target. Even though F contributes to the signal detected by a remote sensor, its magnitude is small (1–5% of the reflected radiation in the near-infrared) thus making the decoupling of the two contributions difficult. Zarco-Tejada et al. (2000a) first recognized the effect of F on r and demonstrated that it is possible to detect the F signal using r measurements. In fact, the reflectance factor usually computed by the RS community as the ratio between upwelling and incident fluxes is indeed polluted by the F contribution:

$$r^*(\lambda) = \frac{\pi L(\lambda)}{E(\lambda)} = r(\lambda) + \frac{\pi F(\lambda)}{E(\lambda)} \quad [-]. \tag{2}$$

This quantity, referred here as apparent reflectance, r^*, differs from the pure reflectance (r) as indicated by the right hand side of Eq. (2) and as shown in Fig. 1B.

Progress in understanding the effect of F in remotely-sensed data have also been made through the development and integration of leaf and canopy F models based on physical methods (Maier, 2000; Olioso et al., 1992; Rosema et al., 1998; Zarco-Tejada et al., 2000a). The FluorMOD canopy F model (Miller et al., 2005) builds on these earlier efforts and provides simulations of incident and reflected radiance and of emitted F by linking three radiative transfer models: MODTRAN-4 for the atmosphere (Berk et al., 1989), FluorMODleaf (Pedrós et al., 2005) for the leaf (based on the PROSPECT model, Jacquemoud & Baret, 1990), and SAIL for the canopy optical properties (Verhoef, 1984, 2005). For a user-friendly interface to the FluorMOD model, the reader is referred to the FluorMODgui tool (Zarco-Tejada et al., 2006) available on line at http://www.ias.csic.es/fluormod.

2. Rationale for passive estimation of *F*

The F signal is comparably stronger and can be detected passively in narrow dark lines of the solar and atmospheric spectrum in which irradiance is strongly reduced (the so-called Fraunhofer lines). In the visible and near-infrared, the solar spectrum at ground level exhibits three main "Fraunhofer" features which have been exploited for F estimation: Hα due to hydrogen (H) absorption in the solar atmosphere (centered at 656.4 nm) and two telluric oxygen (O_2) absorption bands in the Earth atmosphere, O_2-B (687.0 nm) and O_2-A (760.4 nm). The incident at-surface irradiance at different spectral resolutions (0.005, 0.1 and 1.0 nm Full Width at Half Maximum, FWHM) and at the spectral regions around these three absorption features is shown in Fig. 2. Irradiance data were simulated by means of the Matrix Operator Model (MOMO) (Fell & Fischer, 2001). Among other inputs, the sun zenith angle was set to 30°, with a mid-latitude summer atmosphere, the surface at sea level, and the aerosol optical thickness at 550 nm equal to 0.2. Resampling to the different spectral resolutions was performed assuming Gaussian-like spectral response functions with the given FWHM.

Table 1
Characteristics of the three absorption bands most exploited for the remote estimation of F.

Spectral resolution	Hα(Solar)			O_2-B(Telluric)			O_2-A(Telluric)		
	0.005 nm	0.1 nm	1.0 nm	0.005 nm	0.1 nm	1.0 nm	0.005 nm	0.1 nm	1.0 nm
Spectral position[ab] (nm)	656.422	656.463	656.472	687.188	687.032	687.352	760.773	760.417	760.713
Width of darkest well[ac](FWHM, nm)	0.31	0.33	1.26	0.03	0.32	1.54	0.07	0.13	2.80
Depth[ad] (%)	50	47	19	100	57	33	100	92	81
F intensity[e] (W m^{-2} sr^{-1} μm^{-1})	1.9	1.9	1.9	5.0	5.0	5.0	6.0	6.0	6.0
% F with respect to upwelling flux (in)[f]	5	5	3	100	15	10	100	39	22
% F with respect to upwelling flux (out)[f]	2	2	3	7	7	7	5	5	5

The position, width and depth of the features were estimated from the MOMO model simulations (Fell & Fischer, 2001) resampled at three different spectral resolutions (0.005, 0.1 and 1.0 nm). "In" and "out" refer to the wavelength used inside and outside of the relevant absorption band.

[a] Note that O_2 bands are actually composed of a number of smaller absorption features, the darkest of which is utilized to compute position, width and depth.

[b] The wavelength corresponding to the minimum irradiance.

[c] The FWHM is extracted with a Gaussian fitting of the darkest well.

[d] Depth = $100 \cdot [E(\text{out}) - E(\text{in})] / E(\text{out})]$; note that this depth depends on the sun's position and air mass for the O_2 absorption bands.

[e] Indicative values at canopy level from literature review.

[f] Reflectance values of 0.18, 0.18 and 0.35 were assumed in computing the upwelling flux at Hα, O_2-B and O_2-A, respectively.

Fig. 2 shows that the apparent shape of the absorption bands strongly depends on the spectral resolution with which it is observed. In fact, the very narrow features observable with the highest resolution (0.005 nm) at the two telluric bands (O_2-B and O_2-A) are progressively lost when degrading the resolution to 0.1 and 1.0 nm. At O_2-B for example, the FWHM of a single absorption feature goes from 0.03 nm when observed at a 0.005 nm resolution (width of the darkest well of the green curve of Fig. 2) to 1.54 nm when examined with 1.0 nm resolution (blue curve). The same thing occurs for the depth of the band, which is 100% at the highest resolution (i.e., completely dark line, indicating almost no photons reaching the ground) and only 33% at the lowest resolution considered.

As a consequence, band position, width and depth are resolution-dependent features, as reported in Table 1. While these characteristics are not dramatically affected by spectral resolution for Hα, they vary noticeably at the O_2 absorption bands. Note that this discussion was focused on spectral resolution but, in operation, also an insufficient spectral sampling interval (i.e., spacing between sample points in the spectrum) and a systematic shift in the nominal channels position (i.e., shift of the center wavelength) would result in a distortion of the spectral characteristics of the absorption bands.

The O_2 absorption bands were used more extensively than the H feature because, when observed with typical resolutions from a tenth of a nanometer to a few nanometers they appear wider and deeper. Moreover, they are spectrally closer to the peaks of the *F* emission spectrum positioned at about 690 and 740 nm (see Fig. 1) thus making the contribution of *F* to the overall upwelling signal more significant (see Table 1). The main drawbacks associated with the use of the O_2 absorption features for *F* retrieval are that the shape and width of the features are subject to spatial and temporal variations because they depend on the atmospheric state, the illumination and observation geometry, and because the emitted *F* is re-absorbed along the upward atmospheric path which diminishes the signal to be measured by an airborne or spaceborne instrument.

The rationale for the passive estimation of *F* is therefore to exploit these dark bands by measuring to what extent the "wells" are filled by *F* relative to the reflectance *continuum* (Elachi, 1987). For example, at the O_2-A band the incident radiation at ground level is attenuated by up to more than 90% when measured with a resolution of about 0.1 nm (see Table 1). With such a resolution, details of the internal structure and narrow features of the O_2-A band can be observed in the incident solar radiance spectrum collected with a high spectral resolution spectrometer (Fig. 3).

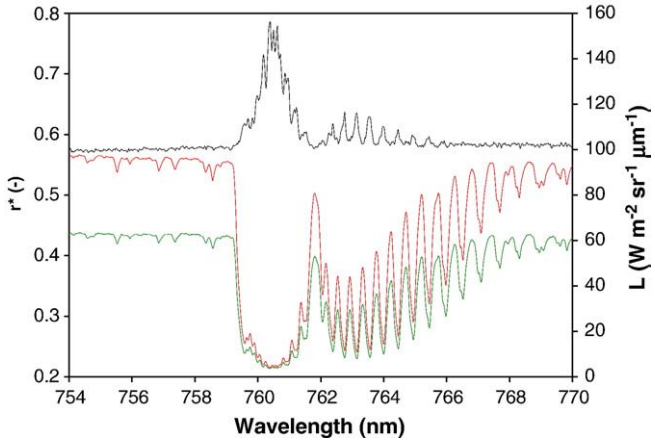

Fig. 3. Apparent reflectance factor (*r**, black curve) at the O_2-A band calculated from incident and upwelling radiances (red and green curves, respectively) over a white clover canopy. Measurements were collected early in the morning with an HR4000 spectrometer (OceanOptics, USA) characterized by a FWHM of 0.13 nm and a sampling interval of 0.02 nm. (For interpretation of the references to colour in this figure legend, the reader is referred to the web version of this article.)

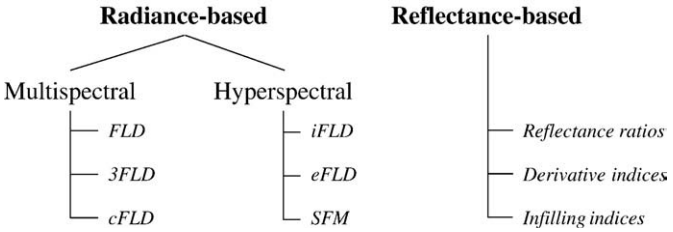

Fig. 4. Classification of *F* retrieval methods according to the RS quantity used (i.e., radiance vs. reflectance) and number of spectral channels (multispectral vs. hyperspectral) and technique employed (techniques and acronyms are defined in the next sections).

Fig. 3 also demonstrates that the reflectance computed as the ratio of the upwelling and downwelling radiances according to Eq. (2) is indeed an apparent reflectance polluted by the *F* contribution from the infilling of the O_2-A band producing the peak at 760 nm. Solar-induced Chl fluorescence affects reflectance outside as well as inside the absorption band, but the proportion of emitted light with respect to the reflected light is higher inside than outside the well, thus causing the appearance of the reflectance peaks for both of the O_2 bands (Fig. 1B) originally observed by Pérez-Priego et al. (2005) and Meroni and Colombo (2006) in their studies of canopy and leaf *F* conducted at sub-nanometer resolution.

It is worth noting that the origin of absorption (solar or telluric) has an impact on operational *F* retrieval. For the telluric O_2 bands, the strength of the atmospheric absorption (e.g., the band depth) is proportional to the air mass the sunlight passes through and is therefore inversely proportional to the cosine of sun zenith angle (SZA), since the higher the sun, the shorter the path through the atmosphere. The same effect occurs when the detector is located at a distance, a factor that becomes critical for airborne and spaceborne sensors. Therefore, photons in the telluric bands are absorbed on their way up from the vegetation through the atmosphere to the remote sensor as well. Consequently, a precise atmospheric correction scheme is required if the sensor is far away from the ground (e.g., sensor located on a satellite, aircraft, or high altitude platform).

Another consequence of the telluric origin of the O_2 bands is that BRDF (Bidirectional Reflectance Distribution Function) effects may affect *F* estimation. Direct and diffuse radiation fields respond to different processes in the atmosphere resulting in atmospheric optical paths with different length and depth of O_2 absorption features. For example, for close-to-nadir illumination conditions, direct radiation from the sun crosses a shorter atmospheric path than diffuse radiation, and it is consequently less absorbed. Miller et al. (2005) observed that this differential absorption in the atmosphere subtly interacts with the canopy BRDF, thus leading to an apparent infilling of the O_2 features when the reflectance factors for direct and diffuse downwelling irradiance are different. The magnitude of these BRDF effects and potential ways of minimizing them are currently under consideration in the development of new models for *F* retrieval.

3. Review of methods used for estimating *F*

Methods used to quantify *F* are divided into two major categories: radiance-based and reflectance-based approaches. The former makes use of radiance measurements (in physical units or instrument counts) and exploits the Fraunhofer line to decouple *F* from the reflected flux. The latter operates with spectral reflectance and does not necessarily require correspondence to a Fraunhofer line. While the radiance-based approach is able to estimate *F*, either in physical or auxiliary units, the reflectance-based approach provides spectral indices which are related to the effect of *F* on *r*. Such spectral indices

derived from reflectance measurements are in some cases not really tracking fluorescence emissions but rather other vegetation physiological effects that are indeed correlated with the same phenomena responsible for fluorescence.

Fig. 4 shows the classification scheme used to catalogue the methods proposed in the literature. Radiance- and reflectance-based approaches are further subdivided according to the number of channels and the technique used to retrieve *F*.

Results of applications of the various methods described in this section are discussed in Section 4.

3.1. Radiance-based approaches

Radiance-based approaches allow *F* estimation in physical units (i.e., radiance units) if the data are radiometrically calibrated. They exploit the narrow absorption feature of a Fraunhofer line and thus make use of high spectral resolution data (from few nanometers up to 0.025 nm of FWHM). Three methods proposed in the literature require 2–3 spectral channels near the investigated absorption line (i.e. FLD, Fraunhofer Line Depth; 3FLD, 3 bands FLD; cFLD, corrected FLD) while three other methods require a set of contiguous channels covering the whole spectral range of interest, a characteristic of hyperspectral data (iFLD, improved FLD; eFLD, extended FLD; SFM, Spectral Fitting Method). According to these spectral requirements, the first and second groups are here referred to as multispectral and hyperspectral methods, respectively.

3.1.1. Multispectral methods

3.1.1.1. FLD. All radiance-based methods found in the literature derive from the Fraunhofer Line Depth (FLD) principle originally proposed by Plascyk (1975) and Plascyk and Gabriel (1975). The FLD relies on two flux measurements, one inside and one outside a Fraunhofer line (for a review of the history and concepts of the FLD see Theisen, 2002). The magnitude of *F* is deduced by comparing the signal measured inside the dark line (λ_{in}, e.g., 687 for O_2-B and 760 for O_2-A) with the signal measured in a nearby wavelength (λ_{out}, e.g., 686 and 758 nm) that contains the entire solar background irradiance.

In practice, the FLD method requires measurement of incident solar irradiance (*E*, Fig. 5A) and target radiance (*L*, Fig. 5B) in λ_{in} and λ_{out} (the bottom and shoulder of the well) to solve the following system of equations:

$$\left.\begin{aligned} L(\lambda_{in}) &= \frac{r(\lambda_{in})E(\lambda_{in})}{\pi} + F(\lambda_{in}) \\ L(\lambda_{out}) &= \frac{r(\lambda_{out})E(\lambda_{out})}{\pi} + F(\lambda_{out}) \end{aligned}\right\}. \tag{3}$$

Solar-induced Chl fluorescence is then computed on the assumption that *r* and *F* remain constant at the two close wavelengths involved in the measurement:

$$\left.\begin{aligned} r &= \frac{L(\lambda_{out}) - L(\lambda_{in})}{E(\lambda_{out}) - E(\lambda_{in})} \cdot \pi \\ F &= \frac{E(\lambda_{out}) \cdot L(\lambda_{in}) - L(\lambda_{out}) \cdot E(\lambda_{in})}{E(\lambda_{out}) - E(\lambda_{in})} \end{aligned}\right\}. \tag{4}$$

These equations form the basis of the FLD method exploited by the majority of studies (see Section 4 and Table 3). This method is simple and requires radiance measurements in only two spectral channels. The main drawback of the method is that, especially for *r* at 687 nm and *F* at 760 nm, the actual values of these two variables are far from being constant (see for example Fig. 1). Therefore, the weakness of this approach lies in the assumption of constant *r* and *F*, which has been questioned by several authors (e.g. Alonso et al., 2008; Gómez-Chova et al., 2006; Meroni & Colombo, 2006; Moya et al., 2006).

3.1.1.2. 3FLD. To overcome the limitations given by FLD assumptions, Maier et al. (2003) proposed the use of three bands to solve Eq. (3). The single reference band (λ_{out}) is replaced by the average of two bands out of the absorption line, at shorter and longer wavelengths compared to the line, respectively. In this way, a virtual radiance is introduced in the system of Eq. (3). Three spectral channels per absorption line are therefore needed for this method, here referred to as 3FLD.

Theoretically, the advantage of this modification is that it implicitly assumes that *r* and *F* vary linearly in the restricted spectral range considered. Therefore, if this assumption holds, the accuracy of this method should be greater than that provided by standard FLD. Despite this conceptual improvement, a drawback of the method may emerge in its application. In fact, on considering for example the spectral shape of the O_2-A absorption band (see the blue curve at 1.0 nm

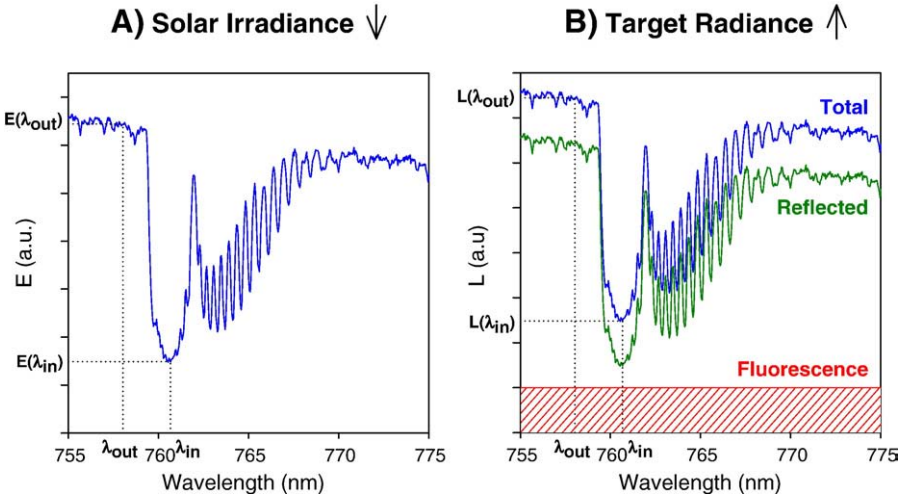

Fig. 5. The standard FLD principle assumes that *r* and *F* are spectrally constant; an example is given at the O_2-A band investigated with a FWHM of 0.13 nm. A): Incident solar irradiance spectrum. B): Upwelling fluxes: the total radiance observed over the vegetated target (blue curve) is made up of the sum of *F* (red area) and pure reflection (green curve). The blue curves in A) and B) are the only measurable quantities. (For interpretation of the references to colour in this figure legend, the reader is referred to the web version of this article.)

resolution in Fig. 2), it is clear that the second reference wavelength (i.e., the one occurring after the absorption line) has to be selected at a wavelength quite far from the well (e.g. >770 nm) in order to avoid the smaller frequency features. The selection of such a wide spectral interval may in turn cause a violation of the underlying assumption of linearity for r and F.

3.1.1.3. cFLD. Gómez-Chova et al. (2006) and Moya et al. (2006) used another variation of FLD (indicated here as cFLD) that employs two correction factors (α_r^* and α_F) in order to account for variations in r and F:

$$r(\lambda_{in}) = \alpha_r^* r(\lambda_{out}), \quad F(\lambda_{in}) = \alpha_F F(\lambda_{out}). \tag{5}$$

At least three bands (one in and two out) are required to compute the r correction factor, α_r^*, which is deduced from apparent reflectance (r^* of Eq. (2)) by interpolating the values obtained outside of the absorption feature. When only two bands outside of the line are available, linear interpolation is used (i.e., linearity is assumed, as in 3FLD). The correction factor for F, α_F, is instead deduced from dedicated measurements of actual F at the leaf level. If only two channels per line are available both correction factors have to be fixed.

It is to be noted that in this method α_r^* is computed by interpolating r^* (i.e., polluted by F) and may not coincide with the actual correction factor for fluorescence-free r. Finally, α_F is assumed to be unique (i.e. fixed independently from the target) and, moreover, has to be known *a priori*. This latter assumption may be violated since α_F can indeed change with F intensity and with different vegetation types (Vila-Francés et al., 2006).

The 3FLD and FLD methods can be considered particular cases of cFLD in which α_F is set to a value of one (3FLD), and both coefficients are set equal to one (FLD).

3.1.2. Hyperspectral methods

3.1.2.1. iFLD. An improved FLD (iFLD, Alonso et al., 2007a, 2008) further refines cFLD by introducing the following developments: *i*) an apparent correction factor for F expressed in terms of measurable quantities and, *ii*) hyperspectral data exploited to interpolate apparent reflectance within the absorption band.

iFLD assumes that the shape of r is similar to that of r^*, once the peak in r^* due to F infilling (as shown in Fig. 3) is removed by means of cubic or spline interpolation which overcomes the cFLD assumption of linearity expressed in Eq. (5). From this interpolated value of r^*, an apparent correction factor (α_r^*) for r is obtained.

After mathematical manipulation of cFLD equations and taking into account that the magnitude of F is always much smaller with respect to the incident solar light out of the absorption line, the correction factor for F was defined as:

$$\alpha_F^* \approx \frac{E(\lambda_{out})}{\tilde{E}(\lambda_{in})} \alpha_r^* \tag{6}$$

where α_F^* and α_r^* are the apparent correction factors for F and r, respectively. $E(\lambda_{out})$ is the irradiance outside the feature, while $\tilde{E}(\lambda_{in})$ is the irradiance within the feature obtained by interpolating the irradiance outside the line to remove the atmospheric absorption effect. The α_F^* factor is defined in such a way that it compensates for the use of α_r^* instead of the real factor (α_r) in the F expression. Eq. (6) therefore introduces a proportionality between the F and r^* correction factors, as both parameters are entangled.

3.1.2.2. eFLD. Another method was proposed by Mazzoni et al. (2007) and named here extended FLD (eFLD). With a spectral resolution of 0.03 nm, they estimated F in the three main absorption bands. With this very high resolution a number of dark lines appear in the incident spectrum instead of one single absorption band (see Fig. 2).

Similar to what has been described for cFLD and iFLD, the eFLD method first reconstructs the apparent reflectance at all the resolved absorption lines present in a single feature (i.e., band). For this purpose it assumes that local maxima in the incident irradiance spectrum correspond to no absorption – which is not always satisfied – and fits r at these local maxima to obtain a continuous reflectance baseline. F is then determined by using this reflectance baseline, according to the following equation:

$$F(\lambda) = L(\lambda) - FIT(r^*(\lambda))E(\lambda)/\pi \tag{7}$$

where $FIT(r^*(\lambda))$ is the fit of the apparent reflectance $r^*(\lambda)$. In this way, an assumption similar to those of iFLD is made on the reflectance function only, while the spectral shape of F is not prescribed.

3.1.2.3. SFM. Spectral Fitting Methods (SFM) are here defined as methods in which both r and F are determined by spectral curve fitting. SFM relaxes the FLD assumptions by employing simple mathematical functions to describe the two key variables (r and F). Differently from the other hyperspectral methods described above, r and F are decoupled in a single step without making use of the apparent reflectance baseline.

Meroni and Colombo (2006) used a SFM in which linear functions were used to describe $r(\lambda)$ and $F(\lambda)$ of Eq. (1) in a restricted spectral range around the two O_2 absorption bands. With a large number of contiguous spectral observations provided by very high spectral resolution spectrometers (e.g., FWHM = 0.1 nm), an overdetermined bilinear system was formed with Eq. (1) and the four unknowns (i.e., gain and offset of the linear $r(\lambda)$ and $F(\lambda)$ functions) were estimated. More recently, Mazzoni et al. (2008) exploited the highest spectral resolution found in the literature (FWHM ~ 0.025 nm) using quadratic functions to represent $r(\lambda)$ and $F(\lambda)$ for the more difficult O_2-B band retrievals.

In summary, the FLD assumptions of constant r and F are replaced by SFM assumptions of linear/quadratic variation of the two variables. Higher order polynomials can be used to represent the two variables, but a detailed study indicating conclusively which mathematical functions would provide the most realistic F estimation at the different absorption bands has yet to be published. Guanter et al. (2009) tested approaches where background reflectance is described as a n-degree polynomial in wavelength, resulting in a second degree polynomial ($n = 2$) for the O_2-A band, while a higher degree polynomial ($n = 6$) was necessary for the O_2-B band, as tested over a large database of many possible combinations of r and F cases. Moreover, the indication of the proper functions must be associated with the definition of their spectral domain. In fact, the validity of the assumptions made by SFM depends on the spectral range to which the method is applied: for example the linearity proposed by Meroni and Colombo (2006) is plausible in the narrow spectral domain used by the authors but may be questionable over wider ranges.

3.2. Reflectance-based approaches

Reflectance-based approaches compute optical indices related to F but cannot provide F estimates in physical or auxiliary units. In fact, these methods exploit the effect of F on the apparent reflectance spectrum in the red-edge region (from 650 to 800 nm). Several indices have been proposed for this purpose (Table 2). Note that these indices were originally derived from hyperspectral data but, with the exception of the indices involving derivatives, most of them require two or three narrow channels only.

Reflectance-based indices can be grouped into three categories (Table 2): reflectance ratios (RR), derivatives (D) and infilling (I) indices.

Table 2
Summary of reflectance-based indices developed for estimating *F*.

References	Device name	Illumination	Scale	Index type	Index formulation
		Artificial/Environmental	Leaf/Canopy	Reflectance Ratio/Derivatives/Infilling	
Ground level					
Zarco-Tejada et al. (2000a)	ST1000 (OceanOptics), Integ. Sphere (Li-Cor), long-pass filter (RG695)	A	L	RR	$(r675 \cdot r690) / r683^2$
				Time difference	$r740_{t1} - r740_{t2}$
				RR	r750 / r800
				RR	r685 / r655
				RR	r690 / r655
Zarco-Tejada et al. (2000b)	CASI (Itres), long-pass filter (RG695)	A	C	RR	r680 / r630
				RR	r685 / r630
				RR/I	r687 / r630
				RR	r690 / r630
				RR	$r685^2 / (r675 \cdot r690)$
				RR	r685 / r655
Zarco-Tejada et al. (2003b)	FieldSpec FR Pro (ASD)	A	C	D/I	$DPI = (D688 \cdot D710) / D697^2$
				D/I	Area of D (688 − 710)
				D	D705 / D722
				D	D730 / D706
				D	DλP / D720
				D	DλP/D(λP + 12 nm)
Dobrowski et al. (2005)	FieldSpec FR Pro (ASD)	A	C	RR	r690 / r600
				RR	r740 / r800
Pérez-Priego et al. (2005)	HR2000 (OceanOptics)	E	C	I	r760.59 − r759.5
Airborne level					
Zarco-Tejada et al. (2000b)	CASI (Itres)	E	C	D	D730/D706
				D	DλP/D703
				RR	$r683^2/(r675 \cdot r691)$
				RR	r685/r655

D is the first derivative of reflectance with respect to wavelength, whereas DλP is the derivative of the reflectance at the inflection point of the red edge. "Time difference" (used for $r740_{t1} - r740_{t2}$) refers to a laboratory method in which the relative magnitude of *F* is deduced from the reflectance difference determined between two times at which *F* is different.

Reflectance ratios do not exploit the Fraunhofer lines but instead use a set of 2–3 spectral reflectances including at least one wavelength affected by *F* (in the neighbourhood of *F* emission maxima, about 685 and 740 nm) and one less or not affected. *F* is then estimated by normalizing the former band by the latter with the aim of removing the spectral information related to the *r* shape (e.g. r690/r600 and r740/r800 proposed by Dobrowski et al., 2005).

Derivative indices are also based on normalization, with the difference that derivatives of reflectance are used instead of reflectances. In fact, Zarco-Tejada et al. (2003b) argued that the effect of *F* on *r* is enhanced by calculation of the derivative reflectance that enables the detection of subtle changes due to *F* emission while minimizing other confusing effects.

The use of normalization and derivatives optimizes these indices to be sensitive to *F*, but a full decoupling from the reflected flux cannot be achieved. Therefore, their application to vegetated targets having different *r* may be problematic.

The last category of indices is infilling, which exploits the existence of Fraunhofer lines. The index r760.5–r759.5 proposed by Pérez-Priego et al. (2005) directly quantifies the infilling effect by measuring the height of the apparent reflectance peak (see Fig. 3). Therefore, this index measures the *F* infilling effect on *r* rather than *F* itself. The strength of the infilling is due to both *F* magnitude and Fraunhofer Line Depth. Since the line depth of the O_2 bands is affected by the sun's position and air density, the analysis of vegetation with this method is limited to a relative comparison of measurements acquired at the same time and under the same observation conditions.

Other indices reported in Table 2 (i.e., r687/r630, and the Double Peak Index, DPI, proposed by Zarco-Tejada et al., 2000b, 2003b) can be regarded as a mixture of the three categories of indices.

In summary, reflectance-based indices first enabled extraction of *F* from traditional RS measurements of *r* and opened the way to further progress and developments. These indices have the advantage of not requiring the complex processing necessary for other methods but have the weakness of providing estimates in relative units related to the effect of *F* on *r*. Moreover, several indices described in Table 2 are not sensitive to changes in *F* alone. Because pigments have distinctive absorption spectra depending on their molecular structure and local chemical environment (Ustin et al., 2006), *r* variations in the red-edge region may be due to both *F* and antenna pigment conformational changes. These changes are linked to *F* and are physiologically relevant, but they are not *F per se*.

Despite this limitation, reflectance-based methods (excluding infilling indices) are often the only methods that allow passive remote measurements of fluorescence in indoor environments where artificial light is used and the radiance-based approaches cannot be applied.

4. Review of devices and applications

In this section we present the development of *F*-sensing capabilities from pioneer works of the 1970s to the current state of the art. Studies conducted at ground, aircraft and satellite levels are listed (Table 3) together with relevant information concerning retrieval method, device used and practical application of the study.

The majority of the research has been performed at ground level, thus exploiting the easier availability of ground-based instruments. The practical goal of most of the works has been to demonstrate the capability of *F*-sensing methods to detect and track plant stress. In many cases, the objective of the research was purely to demonstrate the feasibility of sensing the *F* signal with a given device or method.

Several different devices have been used for estimating *F*, including commercial field spectrometers, in-house developed instruments assembled by several research groups, commercial or research airborne devices and even a satellite sensor.

The name of the variable used to indicate solar-induced Chl fluorescence in each study is reported (Table 3) and shows that different abbreviations have been used to indicate the same physical quantity including *F* (the one adopted in this manuscript), *SIF* (Solar-Induced Fluorescence), *Fs* (Fluorescence Steady state), and *ChF* or *CF* (Chlorophyll Fluorescence).

Table 3
Studies on vegetation *F* estimation with different methods.

Reference	*F* retrieval method				Detector							Application		*F* estimate	
	Approach and method	Channels per line	Assumptions		Commercial/ In-house developed	Filters/ Dispersive element	Channel position (in, out)/range used			FWHM	Device name	Target	Aim of the work	Name of *F*	Measurement units
	L = radiance-based, R = reflectance-based		On *r*	On *F*			Hα (nm)	O_2-A (nm)	O_2-B (nm)	(nm)		Leaf/Canopy			a.u. = auxiliary
			Constant/Linear/Quadratic/ Smooth/A *priori* corr. factor												
Ground level															
McFarlane et al. (1980)	L, FLD	2[a]	C	C	I	F	656.3[a]			n.a.	FLD Mark II (Perkin-Elmer)	C	Stress detection	*aL*	a.u.
Carter et al. (1990)	L, FLD	2[a]	C	C	I	F	656.28[a]			0.7, 1	FLD Mark II (Perkin-Elmer)	L	Plant physiology	*F*	mW m^{-2} nm^{-1}
Carter et al. (1996)	L, FLD	2[a]	C	C	I	F			687[a]	1, 5	FLR	L	*F* sensing	*F*	a.u.
Kebabian et al. (1999)	L, FLD[b]				I	–[b]		762[b]	688[b]	–[b]	PFS	C	*F* sensing + stress detection	*PF*	mW m^{-2} nm^{-1}
Moya et al. (1999)	L, FLD	2	C	C	I	F		760.5, 758.5		1	Bidetector	L	*F* sensing	*F*	a.u.
Evain et al. (2001)	L, FLD	2	C	C	I	F		760, n.a.	687, n.a.	0.5	PMFD	L + C	*F* sensing	*F*	a.u.
Evain et al. (2002)	L, FLD	2	C	C	I	F		760, n.a.	687, n.a.	0.5	PMFD	C	Stress detection	*F*	a.u.
	L, FLD	2	C	C	I	F		760.5, 758.5		1	Bidetector	C	Stress detection	*F*	a.u.
Freedman et al. (2002)	L, FLD[b]				I	–[b]		762[b]	688[b]	–[b]	PFS	C	Stress detection + physiology	–	mW m^{-2} nm^{-1}
Carter et al. (2004)	L, FLD[b]				I	–[b]		762[b]	688[b]	–[b]	PFS	L	Stress detection	*F*	mW m^{-2} nm^{-1}
Moya et al. (2004)	L, FLD	2	C	C	I	F		760.5, 758.5		1	Bidetector	L + C	*F* sensing	*f*[c]	a.u.
Liu et al. (2005)	L, FLD	2	C	C	C	D		760, 756	687, 684	3	FieldSpec FR Pro (ASD)	C	*F* sensing	*f*	W m^{-2} μm^{-1}
Louis et al. (2005)	L, FLD	2	C	C	I	F		760.6, 758.3	687.3, 686.2	1.3, 0.7, 1.6, 0.8	PMFD	C	Plant physiology	*F*	a.u.
Corp et al. (2006a)	L, FLD	2	C	C	C	D		760, n.a.	688, n.a.	3	FieldSpec FR Pro (ASD)	C	Stress detection	*SIF*	mW m^{-2} $sr^{-1}nm^{-1}$
Corp et al. (2006b)	L, FLD	2	C	C	C	D		760, n.a.	688, n.a.	3	FieldSpec FR Pro (ASD)	C	*F* sensing + stress detection	*SIF*	mW m^{-2} $sr^{-1}nm^{-1}$
Middleton et al. (2006a)	L, FLD	2	C	C	C	D		760, n.a.	688, n.a.	3	FieldSpec FR Pro (ASD)	C	Stress detection	*SIF*	mW m^{-2} $sr^{-1}nm^{-1}$
Middleton et al. (2006c)	L, FLD	2	C	C	C	D		760, n.a.	688, n.a.	3	FieldSpec FR Pro (ASD)	C	Stress detection	*SIF*	a.u.
Amorós-López et al. (2008)	L, FLD	2	C	C	C	D		760, n.a.	687, n.a.	3	FieldSpec FR Pro (ASD)	L	*F* sensing + plant physiology	*ChF*	W m^{-2} $sr^{-1}nm^{-1}$
Middleton et al. (2008)	L, FLD	2	C	C	C	D		760, n.a.	688, n.a.	3	FieldSpec FR Pro (ASD)	C	Comparison with model	*SIF*	mW m^{-2} $sr^{-1}nm^{-1}$
Maier et al. (2003)	L, 3FLD	3	L	L	C	D		762, n.a.		2.5	MCS501 (Zeiss Jena GmbH.)	L	*F* sensing	*L fluor.*	mW m^{-2} $sr^{-1}nm^{-1}$
Stellmes et al. (2007)	L, 3FLD	3	L	L	C	D		760, 750, 770		3	FieldSpec FR Pro (ASD)	C	Stress detection	*Fs*	a.u.
Gómez-Chova et al. (2006)	L, cFLD	3	L, based on apparent *r*	A	C	D		760, n.a.	687, n.a.	3	FieldSpec FR Pro (ASD)	L	*F* sensing	*f*	a.u.

Alonso et al. (2008)	L, iFLD	>3	S, based on apparent *r*	S, based on apparent *r*	C	D		761, 754		3	FieldSpec FR Pro (ASD)	C	*F* sensing	*f*	W m^{-2} sr^{-1} μm^{-1}
Mazzoni et al. (2007)	L, eFLD	512	S, based on apparent *r*	–	I	D	~653–668	~758–773	~686–701	0.03	EG&G double monochromator	L	*F* sensing	*F*	a.u.
Meroni et al. (2004)	L, SFM	71 (O_2-B), 118 (O_2-A)	L	L	C	D		759.03–764.04	686.51–690.05	0.2	HR2000 (OceanOptics)	L	*F* sensing	*F*	W m^{-2} sr^{-1} μm^{-1}
Meroni and Colombo (2006)	L, SFM	71 (O_2-B), 118 (O_2-A)	L	L	C	D		759.03–764.04	686.51–690.05	0.2	HR2000 (OceanOptics)	L	*F* sensing	*F*	W m^{-2} sr^{-1} μm^{-1}
Meroni et al. (2008a)	L, SFM	71 (O_2 B), 118 (O_2 A)	L	L	C	D		759.03–764.04	686.51–690.05	0.2	HR2000 (OceanOptics)	L	Stress detection	*Fs*	W m^{-2} $sr^{-1}$$nm^{-1}$
Meroni et al. (2008b)	L, SFM	439	L	L	C	D		759.0–767.8		0.13	HR4000 (OceanOptics)	C	Stress detection	*Fs*	W m^{-2} $sr^{-1}$$nm^{-1}$
Mazzoni et al. (2008)	L, SFM	510	Q	Q	C	C			684.5–689.5	0.025	Double monochromator	L	*F* sensing	*F*/*Smax*[d]	a.u.
Zarco-Tejada et al. (2000a)	R, RR	>3[e]	S	S	C	D		–[e]	–[e]	7.3	ST1000 (OceanOptics)[f]	L	*F* sensing	–[g]	a.u.
Zarco-Tejada et al. (2000b)	R, RR/I	>3[e]	S	S	C	D			–[e]	2.5	CASI (Itres) + Schott RG 695	C	*F* sensing	–[g]	a.u.
Zarco-Tejada et al. (2003b)	R, D/I	>3[e]	S	S	C	D			–[e]	3	FieldSpec FR Pro (ASD)	C	*F* sensing	–[g]	a.u.
Dobrowski et al. (2005)	R, RR	>3[e]			C	D		–[e]	–[e]	3	FieldSpec FR Pro (ASD)	C	Stress detection	Fs	a.u.
Pérez-Priego et al. (2005)	R, I	2	C	C	C	D		–[e]		0.065[h]	HR2000 (OceanOptics)	C	Stress detection	–[g]	a.u.
Airborne level															
Maier et al. (2002)	L, FLD	2	C	C	I	D		762, n.a.		~7	ROSIS (DLR)	L + C	*F* sensing	*Lfluorescence*	a.u.
Maier et al. (2003)	L, FLD	2	C	C	I	D		762, n.a.		~7	ROSIS (DLR)	C	*F* sensing	*Lfluorescence*	a.u.
Zarco-Tejada et al. (2003a)	L, FLD	2	C	C	C	D		762, 754	693, 678	7.5	CASI (Itres)	C	*F* sensing	*F*	a.u.
Corp et al. (2006a)	L, FLD	2	C	C	C	D		760, n.a.	688, n.a.	3	AISA (Specim)	C	Stress detection	*SIF*	mW m^{-2} $sr^{-1}$$nm^{-1}$
Middleton et al. (2006b)	L, FLD	2	C	C	C	D		760, n.a.	688, n.a.	3	AISA (Specim)	C	Comparison with model	*SIF*	mW m^{-2} $sr^{-1}$$nm^{-1}$
Middleton et al. (2007)	L, FLD	2	C	C	C	D		760, n.a.	688, n.a.	3	AISA (Specim)	C	Stress detection	*SIF*	mW m^{-2} $sr^{-1}$$nm^{-1}$
Zarco-Tejada et al. (2009)	L, FLD	2	C	C	C	F		760.47, 757.42		1.57, 1.6	MCA-6 (Tetracam)	C	Stress detection	*F*	W m^{-2} $sr^{-1}$$nm^{-1}$
Moya et al. (2006)	L, cFLD	3	L, based on apparent *r*	A	I	F		760.7,758.2, 770.4	687.3,686.1, 694.3	1.0, 0.5	AIRFLEX (interference filters)	C	*F* sensing	*F*	a.u.
Zarco-Tejada et al. (2000b)	R, RR/I	>3[e]			C	D			–[e]	2.5–7.5	CASI (Itres)	C	*F* sensing	*CF*	a.u.
Spaceborne level															
Guanter et al. (2007)	L, cFLD	2 for *F*, 3 for *r*	L	A	–	D		760.6, 753.8		3.75, 7.5	MERIS (ESA)	C	*F* sensing	*Fs*	W m^{-2} sr^{-1} μm^{-1}

Note that mW m^{-2} sr^{-1} nm^{-1} = W m^{-2} sr^{-1} μm^{-1} and n.a. stands for not available.

[a] Two coincident bands were used, one wider than the other.

[b] The induced fluorescence approach exploiting a low-pressure O_2 cell is used.

[c] *Fs* was used for the fluorescence yield.

[d] *Smax* is the maximum intensity of the source in W m^{-2} cm^{-1}.

[e] The number and spectral position of channels vary in different indices.

[f] The 1800-12 IS (Li-Cor) integrating sphere was used with a Schott RG 695 long-pass filter.

[g] The infilling effect of *F* on *r* is estimated.

[h] Spectral sampling instead of FWHM is reported.

4.1. Ground level

Ground-based measurements allow quantifying of both incident and upwelling radiations which are necessary in using *F* retrieval methods. Incident radiation is usually evaluated by measuring the radiance reflected by a standard reflectance panel (e.g., Spectralon, Labsphere, USA). An atmospheric correction of the measured fluxes is generally not performed since the optical path from the target to the sensor is normally very short (i.e., from centimeters to meters). For a review of the physical basis and practical aspects of field spectroscopy measurements see Milton et al. (2009).

Multispectral methods belonging to the radiance-based approach were exploited in most of the studies found in the literature. Earlier works by McFarlane et al. (1980) and Carter et al. (1990) applied the standard FLD to the Hα line. They used a prototype device named the FLD Mark II described in Plascyk (1975) and Plascyk and Gabriel (1975), a filter-based system designed to operate at any of three Fraunhofer lines: 486.1 nm (Hβ), 589.0 nm (NaD_2) and 656.3 nm (Hα) with a FWHM of 0.07 nm. McFarlane et al. (1980) employed this instrument in the context of a water stress experiment, and were able to discriminate between irrigated and non-irrigated lemon trees from a platform 12 m above the ground. Carter et al. (1990), using a different bandwidth (i.e., 0.7 nm) in a field experiment, found a negative relationship between *F* and net CO_2 assimilation rate in attached leaves of three species.

In a subsequent work, Carter et al. (1996) investigated the O_2-B band with the prototype Fraunhofer Line Radiometer (FLR) instrument. For the first time they used DCMU, an herbicide that blocks electron transport in photosystem II and enhances *F* emission, to test the *F*-sensing capability of their system. They were able to record an enhanced *F* signal for DCMU-treated palm leaves, while no *F* differences between treated and controls were detected for grape leaves. As in the previous works by Carter et al. (1990) and McFarlane et al. (1980), the FLD method was applied to two coincident (overlapping) spectral bands with the same band center but with different bandwidths (narrow vs. wider) instead of two spectrally independent observations (inside and outside the absorption feature). For example, in Carter et al. (1996), both bands were centered at 687 nm while the bandwidths were 1 and 5 nm, respectively. It is evident that the wider band, which should represent the non-absorbed *continuum*, is contaminated by absorption occurring within the absorption feature.

More recently, Moya et al. (1999, 2004), Evain et al. (2001, 2002) and Louis et al. (2005) applied FLD to both O_2 bands using prototype instruments. The Bidetector (Moya et al., 1999, 2004) and its multichannel version, the PMFD (Passive Multi-wavelength Fluorescence Detector, Evain et al., 2001) were developed at LURE-CNRS (France). Both prototypes use interference filters to measure the radiation coming from the target, as well as from a white-reference panel at two wavelengths, one centered at the absorption feature and the other located outside the absorption feature. The Bidetector estimates *F* at the O_2-A band (FWHM = 1 nm), while PMFD works for both the O_2 absorption bands (FWHM = 1.3 nm in the O_2-A band, and 0.7 nm in the O_2-B band). Both instruments provide *F* estimates in arbitrary units.

Evain et al. (2002) successfully used both prototypes to follow physiological modifications of maize plants in response to stress conditions (i.e., DCMU and water stress) from a distance of 7–9 m. Louis et al. (2005) installed the PMFD device on top of a 20 m high tower and used it to track naturally-induced *F* variations and related information on vegetation photosynthetic capacity.

The prototype instrument PFS (Plant Fluorescence Sensor, Kebabian et al., 1999) acts as a Fraunhofer line discriminator but, differently from the previously described devices, operates as an induced fluorescence detector. The light collected from the plant is directed through a cell containing low-pressure O_2 which absorbs and then re-emits photons which are detected by a photomultiplier tube. This allows measurement within the fully dark core of the absorption lines present at the O_2-A and O_2-B features (Fig. 1, irradiance curves at 0.005 nm spectral resolution). As a consequence, the PFS must be close to the plants being measured because atmospheric O_2 also appreciably absorbs *F* along with sunlight in such dark line cores. In nitrogen fertilization experiments, Kebabian et al. (1999) and Freedman et al. (2002) focused their attention on the F687/F760 ratio computed from PFS measurements at canopy level. Plants that have been subjected to nitrogen stress demonstrated a higher ratio than control plants. Freedman et al. (2002) also reported a robust negative linear correlation between the ratio and net CO_2 assimilation. Carter et al. (2004) used the PFS instrument in a herbicide-induced stress experiment at leaf-level (corn and soybean plants treated with bromacil) and recorded an enhanced *F* signal at both the O_2-A and O_2-B bands.

In contrast to the use of in-house developed prototypes, several authors have applied standard FLD to RS data collected by a commercial field spectrometer (i.e., FieldSpec, FS Pro, Analytical Spectral Devices Inc., USA) (Amorós-López et al., 2008; Corp et al., 2006a,b; Liu et al., 2005; Middleton et al., 2006a,c, 2008). The use of such a calibrated spectrometer allowed estimation of *F* in physical units. However, the bandwidth of the instrument (FWHM = 3 nm) is not perfectly suited for *F* estimation, especially at the O_2-B band, because it may include the shoulder spectral regions on either side of the absorption features, a condition that results in an overestimation of *F* (Middleton et al., 2008). This observation is supported by a study conducted at leaf level with an ASD FieldSpec FR Pro by Amorós-López et al. (2008). They estimated *F* using the FLD and simultaneously measured *F* with a special device blocking the incident irradiance with shortpass filters (in the spectral range of *F* emission) so that the upwelling radiance is purely composed of *F*. They found an *F* overestimation by using the FLD method, which was more pronounced at the O_2-B band.

Further indications of inappropriate spectral resolution are found in Gómez-Chova et al. (2006). They tested the use of correction factors (cFLD) to compensate for the spectral shape of the two key variables and were able to reduce the bias and dispersion of *F* estimation for the O_2-A with respect to FLD, while no satisfactory results were achieved at the narrower O_2-B. This was explained by the fact that the spectrometer used (the ASD FieldSpec FR Pro) has sufficient radiometric sensitivity but sub-optimal spectral resolution. However, it is likely that the difficulties in estimating *F* at the O_2-B band are not only related to the resolution but also to the spectral shape of the *r* curve in this region, which is neither as constant as the FLD method assumes nor easy to correct using empirical factors. In fact, a large heterogeneity exists in the correction coefficients, especially the one relating to *r*, as pointed out by Vila-Francés et al. (2006) who studied a number of different species.

Maier et al. (2003) performed ground-based radiance measurements with a Multi-Channel Spectrometer MCS501 (Carl Zeiss Jena GmbH, Jena, Germany) which provides a spectral resolution of 2.5 nm and estimated *F* with the 3FLD applied to the O_2-A absorption band. The central wavelength for the line was selected at 762 nm and the wavelength channels before and after this were used as references. They compared the Kautsky induction kinetic of *F* estimated with the 3FLD on dark-adapted leaves after the onset of continuous illumination with the fluorescence measured with a Pulse Amplitude Modulated fluorometer (PAM-2000, Walz, Germany). They observed almost identical steady-state fluorescence values after about 1 min and very similar induction kinetics except for the very beginning of the illumination period because different portions of the broad-leaved dock plant were measured by the two instruments: MCS501 views 300 cm^2 or almost the entire plant, while the PAM-2000 views only 0.3 cm^2. Stellmes et al. (2007) estimated *F* from ASD FieldSpec FR Pro data gathered at canopy level with the 3FLD applied to the O_2-A absorption band. The radiance outside the band was calculated

averaging the 750 and 770 nm bands, while the radiance inside was measured at 760 nm. In the context of a drought stress experiment, they showed that *F* dissipation was connected to photosynthetic rate and observed that light- to medium stress led to a decrease in *F* due to an increase in heat dissipation.

Applications of radiance-based hyperspectral methods were also found in several studies. The iFLD method applied at the O_2-A band was tested at canopy level by Alonso et al. (2008) on a simulated database and a large set of ASD FieldSpec FR Pro measurements. The authors found that FLD overestimates *F* while iFLD is able to reduce this bias. With a sensitivity analysis it was also demonstrated that any FLD-based method is more sensitive to inaccuracies in the determination of α_r (i.e., determining true *r*) than to those of α_F. This finding is in agreement with the observation that most of the flux upwelling from a vegetated target is controlled by the reflected component which, if not accurately modelled, results in a large error in *F* estimation.

Mazzoni et al. (2007) presented preliminary results of the eFLD method that exploits the highest resolution found in the literature (FWHM ~ 0.025 nm) which was provided by a double monochromator (EG&G, USA). Besides the *F* value, they were able to estimate its shape at the different spectral windows considered in the study (Hα and both O_2 bands).

The SFM was first used at leaf level by Meroni et al. (2004) and Meroni and Colombo (2006) at both the O_2 absorption bands in the framework of a DCMU treatment experiment. High spectral resolution data (~0.2 nm FWHM) collected with commercial spectrometers (HR2000, OceanOptics, USA) were used to fit a linear model for both *r* and *F*. Results of this work were consistent at the O_2-A band, where use of the SFM allowed estimation of a negative slope for the emission spectrum at 760 nm. The SFM also enabled the prediction of the wavelength at which *F* was reduced to zero, estimated to occur (on average) at 787 nm, in agreement with leaf emission spectra produced by actively-induced fluorescence methods. Part of the variance in the upwelling radiance was not explained by the model at the O_2-B band, thus indicating that the assumption of linearity may not be suitable in this spectral region, in agreement with the results of Gómez-Chova et al. (2006). The SFM has been applied at both leaf and canopy levels in ozone stress detection experiments (Meroni et al., 2008a,b) using HR4000 spectrometers (OceanOptics, USA) with a FWHM of 0.13 nm. These experiments demonstrated that the different physiological status between healthy and stressed samples was clearly discriminated by *F* at both leaf and canopy levels before visual symptoms of stress or changes in traditional vegetation indices occurred.

With a higher spectral resolution (FWHM ~ 0.025 nm) and employing a SFM with quadratic functions to describe the two key variables, Mazzoni et al. (2008) estimated *F* at leaf level using a double monochromator. An interesting practical result of this work was that without making use of a radiance and wavelength calibrated instrument they were able to estimate *F* in physical units. The instrumental characterization needed to achieve this result was derived from the comparison of the measured raw incident irradiance spectrum with a modelled one (high resolution MARC radiative transfer code, Carli et al., 2007).

In contrast to the use of the radiance-based approaches described thus far, several studies have exploited the reflectance-based approach. For the first time, Zarco-Tejada et al. (2000a,b), using both model simulation and experimental data, demonstrated that effects of Chl fluorescence are observable in the red-edge spectral region of apparent reflectance. Moreover, Zarco-Tejada et al. (2000a) extracted the Chl fluorescence spectrum of a leaf from reflectance measurements using two different approaches. The first approach utilized a longpass filter blocking the incident light below 700 nm to avoid fluorescence excitation. The reflectance measured in this way (not polluted by fluorescence) was then compared to the apparent reflectance measured without the filter to deduce the fluorescence spectrum. In the second approach, the fluorescence spectrum of a dark-adapted leaf was computed from the comparison between two reflectance measurements taken at the beginning and end of a sudden and prolonged illumination period that exploited the change in fluorescence amplitude subsequent to exposure (i.e., the Kautsky effect).

Experiments were not conducted outdoors but in growth chambers under artificial illumination (i.e., in the absence of natural Fraunhofer lines). Several reflectance indices in the red-edge region were demonstrated to be capable of tracking the variation of fluorescence as measured by the PAM-2000 (Table 2). Further experiments at leaf and canopy level reported in Zarco-Tejada et al. (2003b) demonstrated that steady-state chlorophyll fluorescence effects are observable in derivative reflectance curves through a double-peak feature in the 690–710 nm spectral region. The best correlations with steady-state chlorophyll fluorescence measurements obtained with the PAM-fluorometer were found for DPI and for the area of the double-peak feature. In addition, Dobrowski et al. (2005) worked in a controlled environment under artificial light and successfully used basic reflectance indices (e.g., r690/r600 and r740/r800) to track changes in fluorescence in response to heat and water stress. Transfer of these methods to operational conditions (i.e., sun illumination and natural canopies) would require additional analysis of canopy structure and bidirectional reflectance effects, as suggested by Zarco-Tejada et al. (2003b). Moreover, the information content of some of such indices must be interpreted with caution, as the observed correlation with fluorescence changes may be induced by spurious correlations generated by the underlying physiology.

Under natural illumination, Pérez-Priego et al. (2005) used a very high spectral resolution spectrometer (HR2000, Ocean Optics, USA) with a spectral sampling of 0.065 nm to estimate the *F* infilling effect at the O_2-A band using the reflectance-based index, r760.59–r759.5 (i.e., amplitude of the apparent reflectance peak). Application of the index was successful in a field test where the authors were able to separate water stress treatments on orchard trees with measurements acquired nearly contemporaneously.

4.2. Airborne and spaceborne levels

Compared with ground-based instruments which provide point measurements, airborne and spaceborne sensors described in this section are (in most cases) imaging spectrometers that provide additional information related to the spatial pattern of *F* in the acquired scene.

However, in contrast to ground-based applications, the quantitative estimation of *F* from air or spaceborne sensors is complicated by the fact that the *F* signal, coupled to the one reflected by the target and the atmosphere's path radiance, is absorbed by the intervening atmosphere en route to the sensor. Therefore, the increase in the ratio between emitted and reflected radiation inside absorption features achieved at ground level is less evident. Sophisticated approaches dealing with accurate atmospheric and instrumental modelling have yet to be developed for the retrieval of *F* following radiance-based approaches. Until now, empirical approaches have often been used for this purpose, while only a few studies have performed atmospheric corrections using radiative transfer codes.

Maier (2001) first proposed a semi-empirical atmospheric correction scheme for the application of FLD at the O_2-A band which requires non-fluorescing pixels to be present in the scene. The correction takes into account the atmospheric effect on the radiance reaching an airborne sensor, including the atmospheric transmission and path radiance in the algorithm. This method was tested on reflectance spectra measured on the ground and simultaneously acquired by the ROSIS (Reflective Optics System Imaging Spectrometer) airborne spectrometer (DLR, Germany) operating with 4 nm spectral sampling and ~7 nm FWHM at the Barrax study site in central Spain (Maier

et al., 2002, 2003). On analyzing the spatial patterns of *F* provided by the imaging spectrometer, the authors concluded that *F* gives information different from that of spectral vegetation indices, thus supporting the hypothesis that additional insights into photosynthesis and plant stress can be gathered from *F* estimated from airborne observations.

Zarco-Tejada et al. (2003a) investigated the possibility of detecting *F* at both O_2 absorption bands from hyperspectral CASI (Compact Airborne Spectrographic Imager, Itres, Canada) data operating with bands having a 7.5 nm FWHM. Using the FLD method and the atmospheric correction scheme of Maier (2001) and Maier et al. (2002), they studied corn crops grown under different stress conditions due to different nitrogen treatments. Although the spectral resolution appears inadequate for the estimation of *F*, especially at the O_2-B band, the authors reported a satisfactory correlation between canopy CASI-derived canopy *F* and ground-truth leaf measurements of fluorescence using a Lidar system. More recently, Zarco-Tejada et al. (2009), applied the same method to detect water stress in orchard trees (peach, orange and olive). In this work, airborne imagery was acquired by a multispectral camera (MCA-6, Tetracam, USA) equipped with bandpass filters providing two narrow-band channels (FWHM ~ 1.6 nm) centered at 760.47 and 757.42 nm for the characterization of the O_2-A absorption feature. The camera, mounted on an unmanned aerial vehicle (UAV) platform, was used to map *F* with very high spatial resolution (15 cm pixel resolution) and discriminate well-watered trees from water-stressed ones (showing lower *F*). Crown level *F* correlated well with both ground-based measurements of PAM-fluorometer steady-state fluorescence and leaf level net CO_2 assimilation rate.

Contributions to *F* retrieval from airborne data are also presented in Corp et al. (2006a) and Middleton et al. (2006b, 2007). In these works, airborne data were acquired by the AISA airborne imaging spectrometer (Specim, Finland) providing a spectral resolution of about 3 nm. The standard FLD method was applied, but data were not corrected for atmospheric effects at either of the O_2 bands. Corp et al. (2006a) obtained *F* intensities in physical units on the same orders of magnitude as those obtained by other works and were able to discriminate corn fields grown with different nitrogen supplies by exploiting the fluorescence ratio F688/F760. Middleton et al. (2006b) used FLD with canopy spectra acquired using both the ground-based ASD FieldSpec FR Pro and the airborne AISA sensor. They observed that the ratio F688/F760 differed greatly when estimated using different data, with airborne estimates 10 times lower than ground-based measurements. Ground observations were consistent with FluorMOD simulations (Pedrós et al., 2005; Verhoef, 2005), thus suggesting that airborne estimates may be in error, most likely because no atmospheric correction was applied in this work.

The cFLD method was applied to the prototype instrument AIRFLEX (Moya et al., 2006) developed in the framework of the Earth Observation Preparatory Programme of ESA. AIRFLEX is a non-imaging (i.e., a targeting instrument) airborne sensor based on interference filters working at both the O_2 bands. Each band is characterized by three channels: one at the absorption peak (i.e., 687.3 and 760.7 nm) and two immediately before (686.1 and 758.2 nm) and after (694.3 and 770.4 nm) the absorption feature, thus allowing interpolation of the reflectance within the band. The FWHM for the O_2-B band was 0.5 nm and 1.0 nm for the O_2-A band. The atmospheric effects were accounted for by means of the Modtran4 model. A second sensor (TERFLEX) identical to AIRFLEX but operated on the ground at the time of the flights was used to provide data for calibration and validation (Daumard et al., 2007). A sensitivity analysis was conducted to evaluate the effects of different flight altitudes (from 300 to 3000 m above ground level) on the band depth in order to guarantee the reproducibility of *F* estimations. Good results were obtained on the depth of both bands for the range of altitudes considered in this case.

The reflectance-based approach was also applied to airborne RS hyperspectral data. Experiments with the CASI sensor were conducted by Zarco-Tejada et al. (2000b) to investigate the ability to detect *F* from an airborne sensor. In this study the authors scaled leaf-level relationships between *r*-based indices and active fluorescence measurements to the canopy level through optically thick vegetation (infinite reflectance) formulae and through canopy radiative transfer models. Results showed that *r*-based indices (e.g., DλP/D703, and $r683^2/(r675*r691)$) were related to the maximum photochemical efficiency of dark-adapted samples F_v/F_m measured by the PAM-2000. In a subsequent paper (Zarco-Tejada et al., 2001) focusing on the study of the effect of *F* on the canopy reflectance signature under natural illumination, small variations in CASI reflectance collected at different times of the day were observed, with the maximum effect occurring at 700 nm. However, a quantitative relationship between *F* and reflectance indices was not established.

Finally, Theisen (2002) and Sioris et al. (2003) investigated the potential of *F* detection from space with model simulations and concluded that the signal can be sensed from an orbiting spectrometer. However, the only study conducted using a spaceborne instrument to estimate *F* over terrestrial ecosystems was performed by Guanter et al. (2007) who used data acquired by the MERIS sensor on board the ENVISAT satellite. MERIS was selected because of its good characterization of the O_2-A absorption feature. In particular, the cFLD was applied to MERIS bands 10 and 11 (centers = 753.8 and 760.6 nm; bandwidths = 7.5 and 3.75 nm, respectively). The *F* retrieval was coupled to an atmospheric correction scheme and validation of MERIS-derived *F* was carried out by comparing it with the retrieval from airborne CASI data at 3 m spatial resolution, which in turn was compared with ground-based measurements. MERIS-derived *F* correlated well with airborne and ground-based estimates, thus proving for the first time that also spaceborne estimation of *F* is feasible.

5. Range of variation of *F* under natural daylight conditions

In order to provide an overview of the results of experiments aimed at *F* estimation, we present a comparison of *F* estimates on different vegetation types, at different observation levels and using different techniques and devices. This comparison was possible for those studies providing *F* in absolute units (less than half of the total number of studies reviewed). The ranges of *F* variation in the O_2-A and O_2-B bands extrapolated from papers providing estimates in physical units are reported in Fig. 6, along with the associated range of incident PPFD (Photosynthetic Photon Flux Density) when available.

Solar-induced Chl fluorescence estimates at the O_2-A band made with different instruments under different illumination intensities vary from near 0 to 17 W m^{-2} sr^{-1} μm^{-1}, while at the O_2-B band values range from near 0 to 36 W m^{-2} sr^{-1} μm^{-1}. These ranges encompass minimum and maximum published values and therefore also include extreme values, including very high values that are unrealistic under natural solar-illumination conditions. The range of variation may be attributed to several factors, such as the investigation type (leaf or canopy), vegetation characteristics (e.g. species, canopy structure, phenology, presence of stress factors), or illumination intensity during data acquisition (i.e. incident PPFD).

Besides these intrinsic factors that modulate the *F* emission, the spectral resolution and method used affect the estimated intensity. In particular, the accuracy of *F* retrieval using the FLD method with ASD data (used in most of papers) is uncertain because the 3 nm bandwidth may include the shoulder spectral regions on either side of the oxygen absorption bands, a condition that would elevate the retrieval estimate (Middleton et al., 2008). In addition, the width of the O_2-B band is narrower than that of the A band (Table 1), and thus the *F* retrieval at the O_2-B band may suffer to a greater extent from the low spectral resolution of the ASD. The idea of a spectral resolution-dependent bias is further supported by the fact that lowest *F* values

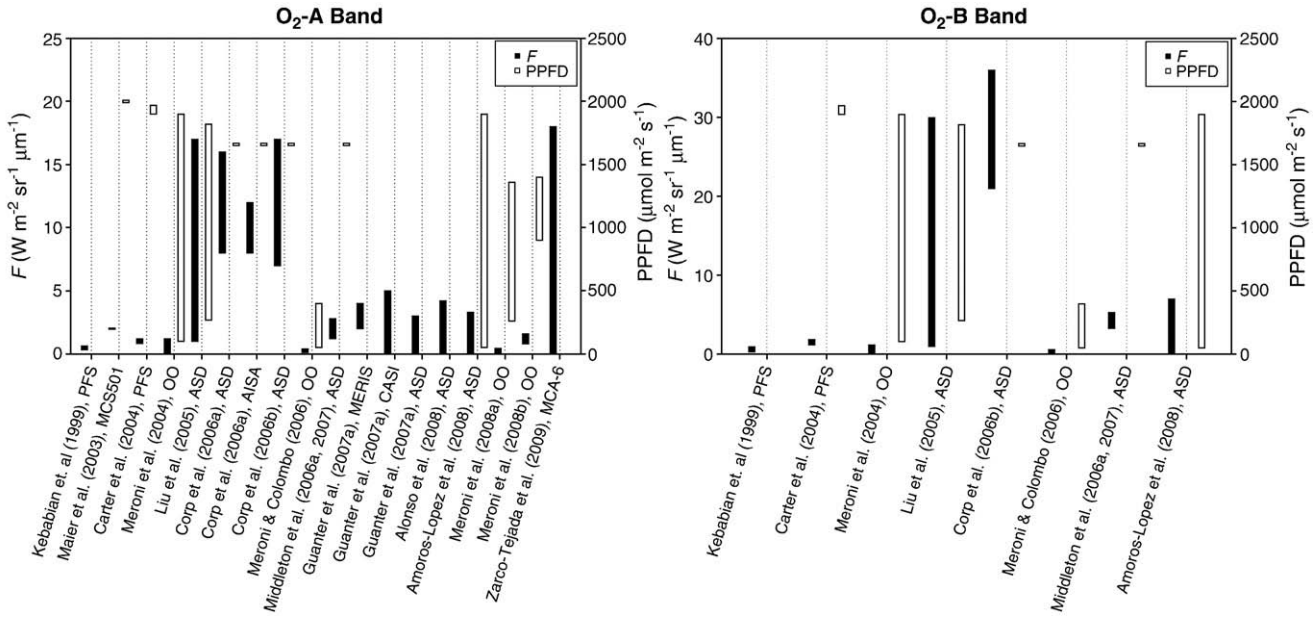

Fig. 6. Ranges of variation (min–max) of *F* in the O_2-A (left) and O_2-B (right) bands extrapolated from published papers providing estimates in physical units. *F* is expressed in W m^{-2} sr^{-1} μm^{-1}. Full bars refer to *F* estimation; empty bars refer to the incident PPFD expressed in µmol m^{-2} s^{-1}. The instrument used is reported in the label, after the reference. Details of the various works can be found in Table 3.

were found in the works of Meroni and Colombo (2006) and Meroni et al. (2004, 2008a,b) which, compared to the other works, exploited a higher spectral resolution (Table 2). Low *F* values were also reported by Kebabian et al. (1999) and Carter et al. (2004) using the induced fluorescence PFS device which acts as a line discriminator with a very high spectral resolution.

Moreover, the method used to estimate *F* may have an impact on this bias, as demonstrated by Alonso et al. (2008), who showed that overestimation (up to one order of magnitude) by the standard FLD method is intrinsic to the hypotheses from which it is formulated, independent of the instrument used. This work also showed that the error in *F* estimation is the consequence of uncertainty of the shape of the true *r*, which has a larger impact on the O_2-B band, where *r* is more variable and difficult to model.

Few works have provided an estimate of *F* in physical units in the Hα band. Carter et al. (1990) reported *F* values between 1.2 and 2.5 W m^{-2} sr^{-1} μm^{-1} for *Zea mays* L. (corn) and *Liquidambar styraciflua* L. (sweet gum). Other values reported in the literature for Hα were gathered with laser excitation, and in most cases using UV excitation. In such cases the amount of fluorescence is not the same as for natural solar illumination. The values reported by Corp et al. (2006b), Louis et al. (2006), and Middleton et al. (2008) were calculated for normalized solar-illumination conditions, and thus are more realistic for the comparison with *F* measurements. Louis et al. (2006) reported values in physical units of fluorescence yield (nm^{-1}) which are adequate for intercomparison of values measured under different levels of illumination.

6. Summary and outlook

Measuring vegetation fluorescence remotely is an appealing prospect but also a challenging one. In this manuscript we review progress towards this goal and we make a first attempt at classifying the different retrieval approaches in some major groups. A rule of thumb to address the best method for estimating *F* cannot be given here for two reasons. First, an assessment of the estimation error of the various methods is missing. This lack of validation is due to the fact that *F* cannot be measured independently on real vegetated targets but can only be estimated. Without actual measurements for use as a benchmark for model validation, estimation accuracy cannot be determined. Second, the choice of a particular method is often in practice restricted by the instrument available. This is why we highlight instrumental requirements as well as the strengths and weaknesses of each approach. For more standardized application of *F* sensing a comparison of the different methods on single case studies is needed. RS data collected for this purpose should be at very high spectral resolution (0.05–0.1 nm), so as to allow subsequent resampling at the desired resolution and application of the whole set of *F* estimation methods, from multispectral to hyperspectral algorithms.

The review of the devices utilized for *F* studies shows that several different instruments were successfully used, including prototypes developed for the purpose of *F* estimation by different research groups and commercial instruments intended for general RS applications. It is interesting to note that today ground-based estimation of *F* can be achieved by several commercially available field spectrometers while there is still a need for technical development in airborne and spaceborne sensors to better fit the spectral requirements for precise *F* retrieval.

This is the main rationale behind the FLEX mission proposal: to implement a satellite mission specifically intended for the most accurate *F* retrieval at several points of the emission spectrum, namely around the O_2-A and O_2-B absorption windows on an operational basis, so that temporally and spatially resolved maps of *F* can be derived from space in order to constrain dynamic vegetation models.

Compared with accepted strategies for vegetation monitoring from optical RS data, the early stage of the research in *F* estimation is evident. In fact, the goal of several studies was limited to demonstrations of the *F*-sensing capability for a given method/device. Nevertheless, other applications, ranging from stress detection to estimation of plant photosynthesis, show that *F* may be fruitfully employed to monitor plant status together with traditional RS reflectance data.

Acknowledgments

This work has been made possible by the funding support of the ESA-project FLEX Performance analysis and requirements consolidation study, through ESTEC contract no. 21264/07/NL/FF. The authors would like to thank the four anonymous reviewers of this manuscript for their valuable comments which have helped us to improve the completeness and overall quality of the paper.

References

Alonso, L., Gómez-Chova, L., Vila-Francés, J., Amorós-López, J., Guanter, L., Calpe, J., et al. (2007). Sensitivity analysis of the Fraunhofer Line Discrimination method for the measurement of chlorophyll fluorescence using a field spectroradiometer. *Geoscience and Remote Sensing Symposium* (pp. 3756–3759). IGARSS 2007.

Alonso, L., Gómez-Chova, L., Vila-Francés, J., Amorós-López, J., Guanter, L., Calpe, J., et al. (2007). Sensitivity analysis of the FLD method for the measurement of chlorophyll fluorescence using a field spectroradiometer. *Proceedings of the 3rd International Workshop on Remote Sensing of Vegetation Fluorescence, Florence, Italy, 7–9 February 2007*.

Alonso, L., Gómez-Chova, L., Vila-Francés, J., Amorós-López, J., Guanter, L., Calpe, J., et al. (2008). Improved Fraunhofer Line Discrimination method for vegetation fluorescence quantification. *IEEE Geoscience and Remote Sensing Letters*, *5*(4), 620–624.

Amorós-López, J., Gómez-Chova, L., Vila-Francés, J., Alonso, L., Calpe, J., Moreno, J., et al. (2008). Evaluation of remote sensing of vegetation fluorescence by the analysis of diurnal cycles. *International Journal of Remote Sensing*, *29*, 5423–5436.

Baker, N. R. (2008). Chlorophyll fluorescence: A probe of photosynthesis in vivo. *Annual Reviews — Plant Biology*, *59*, 89–113.

Baret, F., Houlès, V., & Guérif, M. (2007). Quantification of plant stress using remote sensing observations and crop models: The case of nitrogen management. *Journal of Experimental Botany*, *58*, 869–880.

Berk, A., Bernstein, L. S., & Robertson, D. C. (1989). MODTRAN: A moderate resolution model for LOWTRAN 7. *Air Force Geophysics Laboratory Technical Report GL-TR-89-0122, Hanscom AFB, MA*.

Carli, B., Bazzini, G., Castelli, E., Cecchi-Pestellini, C., Del Bianco, S., Dinelli, B. M., et al. (2007). MARC: A code for the retrieval of atmospheric parameters from millimeter-wave limb. *Journal of Quantitative Spectroscopy and Radiative Transfer*, *105*(3), 476–491.

Carter, G. A., Freedman, A., Kebabian, P. L., & Scott, H. E. (2004). Use of a prototype instrument to detect short-term changes in solar-excited leaf fluorescence. *International Journal of Remote Sensing*, *25*, 1779–1784.

Carter, G. A., Jones, J. H., Mitchell, R. J., & Brewer, C. H. (1996). Detection of solar-excited chlorophyll and fluorescence and leaf photosynthetic capacity using a Fraunhofer line radiometer. *Remote Sensing of Environment*, *55*, 89–92.

Carter, G. A., Theisen, A. F., & Mitchell, R. J. (1990). Chlorophyll fluorescence measured using the Fraunhofer line–depth principle and relationship to photosynthetic rate in the field. *Plant, Cell & Environment*, *13*, 79–83.

Corp, L. A., Middleton, E. M., Daughtry, C., & Campbell, P. K. E. (2006). Solar-induced fluorescence and reflectance sensing techniques for monitoring nitrogen utilization in corn. *Geoscience and Remote Sensing Symposium* (pp. 2267–2270). IGARSS 2006.

Corp, L. A., Middleton, E. M., McMurtrey, J. E., Campbell, P. K. E., & Butcher, L. M. (2006). Fluorescence sensing techniques for vegetation assessment. *Applied Optics*, *45*, 1023–1033.

Daumard, F., Goulas, Y., Ounis, A., Pedros, R., & Moya, I. (2007). Atmospheric correction of airborne passive measurements of fluorescence. *Proceedings of the 10th International Symposium on Physical Measurements and Signatures in Remote Sensing, ISPMSRS'07, Davos, Switzerland, 12–14 March 2007*.

Dobrowski, S. Z., Pushnik, J. C., Zarco-Tejada, P. J., & Ustin, S. L. (2005). Simple reflectance indices track heat and water stress-induced changes in steady-state chlorophyll fluorescence at the canopy scale. *Remote Sensing of Environment*, *97*, 403–414.

Elachi, C. (1987). *Introduction to the physics and techniques of remote sensing* (pp. 63). John Wiley and Sons.

Entcheva Campbell, P. K., Middleton, E. M., Corp, L. A., & Kim, M. S. (2008). Contribution of chlorophyll fluorescence to the apparent vegetation reflectance. *Science of the Total Environment*, *404*, 433–439.

Evain, S., Camenen, L., & Moya, I. (2001). Three-channel detector for remote sensing of chlorophyll fluorescence and reflectance from vegetation. In M. Leroy (Ed.), *8th International Symposium: Physical Measurements and Signatures in Remote Sensing* (pp. 395–400). Aussois, France: CNES.

Evain, S., Ounis, A., Baret, F., Goulas, Y., Louis, J., Cerovic, Z. G., et al. (2002). Passive vegetation fluorosensing using atmospheric oxygen absorption bands. In J. A. Sobrino (Ed.), *Recent advances in quantitative remote sensing* (pp. 509–513). Spain: Publicacions de la Universitat de València.

Fell, F., & Fischer, J. (2001). Numerical simulation of the light field in the atmosphere–ocean system using the matrix-operator method. *Journal of Quantitative Spectroscopy and Radiative Transfer*, *69*, 351–388.

Freedman, A., Cavender-Bares, J., Kebabian, P. L., Bhaskar, R., Scott, H., & Bazzaz, F. A. (2002). Remote sensing of solar-excited plant fluorescence as a measure of photosynthetic rate. *Photosynthetica*, *40*, 127–132.

Gómez-Chova, L., Alonso, L., Amorós-López, J., Vila-Francés, J., del Valle-Tascón, S., Calpe, J., et al. (2006). Solar-induced fluorescence measurements using a field spectroradiometer. Earth observation for vegetation monitoring and water management. *AIP Conference Proceedings*, *852*, 274–281.

Guanter, L., Alonso, L., Gómez-Chova, L., Amorós-López, J., Vila-Francés, J., & Moreno, J. (2007). Estimation of solar-induced vegetation fluorescence from space measurements. *Geophysical Research Letters*, *34*. doi:10.1029/2007GL029289.

Guanter, L., Segl, K., Kaufmann, H., Verhoef, W., Gomez-Chova, L., Alonso, L., et al. (2009, January). Atmospheric corrections for fluorescence signal retrieval. *Final Report ESA—ESTEC Contract 20882/07/NL/LvH*.

Jacquemoud, S., & Baret, F. (1990). PROSPECT: A model of leaf optical properties spectra. *Remote Sensing of the Environment*, *34*, 75–91.

Kebabian, P. L., Theisen, A. F., Kallelis, S., & Freedman, A. (1999). A passive two-band sensor for sunlight-excited plant fluorescence. *Review of Scientific Instruments*, *70*, 4386–4393.

Liu, L., Zhang, Y., Wang, J., & Zhao, C. (2005). Detecting solar-induced chlorophyll fluorescence from field radiance spectra based on the Fraunhofer Line principle. *IEEE Transactions on Geoscience and Remote Sensing*, *43*, 827–832.

Louis, J., Cerovic, Z. G., & Moya, I. (2006). Quantitative study of fluorescence excitation and emission spectra of bean leaves. *Journal of Photochemistry and Photobiology. B, Biology*, *85*(1), 65–71.

Louis, J., Ounis, A., Ducruet, J. M., Evain, S., Laurila, T., Thum, T., et al. (2005). Remote sensing of sunlight-induced chlorophyll fluorescence and reflectance of Scots pine in the boreal forest during spring recovery. *Remote Sensing of Environment*, *96*, 37–48.

Maier, S. W. (2000). Modeling the radiative transfer in leaves in the 300 nm to 2.5 mm wavelength region taking into consideration chlorophyll fluorescence—the leaf model SLOPE. Ph.D. Dissertation, Technische Universität München, München, Germany, 124pp.

Maier, S. W. (2001). Method of deriving sunlight induced fluorescence from radiance measurements and devices for executing the method. United States Patent 6329660.

Maier, S. W., Günther, K. P., & Stellmes, M. (2002). Remote sensing and modelling of solar induced fluorescence. *Proceedings of the 1st Workshop on Remote Sensing of Solar Induced Vegetation Fluorescence, ESTEC, Noordwijk, The Netherlands, 19–20 June 2002*.

Maier, S. W., Günther, K. P., & Stellmes, M. (2003). Sun-induced fluorescence: A new tool for precision farming. In T. VanToai, D. Major, M. McDonald, J. Schepers, & L. Tarpley (Eds.), *Digital imaging and spectral techniques: Applications to precision agriculture and crop physiology* (pp. 209–222). Madison: American Society of Agronomy.

Mazzoni, M., Agati, G., Del Bianco, S., Cecchi, G., & Mazzinghi, P. (2007). High resolution measurements of solar induced chlorophyll fluorescence in the Fraunhofer Hα and in the atmospheric oxygen lines. *Proceedings of the 3rd International Workshop on Remote Sensing of Vegetation Fluorescence, Florence, Italy, 7–9 February 7–9 2007*.

Mazzoni, M., Falorni, P., & Del Bianco, S. (2008). Sun-induced fluorescence retrieval in the O_2-B atmospheric absorption band. *Optics Express*, *16*(10), 7014–7022.

McFarlane, J. C., Watson, R. D., Theisen, A. F., Jackson, R. D., Ehrler, W. L., Pinter, P. J., Jr., et al. (1980). Plant stress detection by remote measurement of fluorescence. *Applied Optics*, *19*, 3287–3289.

Meroni, M., & Colombo, R. (2006). Leaf level detection of solar induced chlorophyll fluorescence by means of a subnanometer resolution spectroradiometer. *Remote Sensing of Environment*, *103*, 438–448.

Meroni, M., Colombo, R., & Cogliati, S. (2004). High resolution leaf spectral signature for the detection of solar induced chlorophyll fluorescence. *Proceedings of the 2nd ESA Workshop on Remote Sensing of Solar Induced Vegetation Fluorescence, Montreal, Canada, 17–19 November 2004*.

Meroni, M., Picchi, V., Rossini, M., Cogliati, S., Panigada, C., Nali, C., et al. (2008). Leaf level early assessment of ozone injuries by passive fluorescence and PRI. *International Journal of Remote Sensing*, *29*, 5409–5422.

Meroni, M., Rossini, M., Picchi, V., Panigada, C., Cogliati, S., Nali, C., et al. (2008). Assessing steady-state fluorescence and PRI from hyperspectral proximal sensing as early indicators of plant stress: The case of ozone exposure. *Sensors*, *8*, 1740–1754.

Middleton, E. M., Corp, L., Daughtry, C., & Entcheva Campbell, P. K. (2006). Chlorophyll fluorescence emissions of vegetation canopies from high resolution field reflectance spectra. *Geoscience and Remote Sensing Symposium* (pp. 4064–4067). IGARSS 2006.

Middleton, E. M., Corp, L. A., & Entcheva Campbell, P. K. (2006). A comparison of measurements and FluorMOD simulations for solar induced chlorophyll fluorescence and reflectance of a corn crop under nitrogen treatments. In J. A. Sobrino (Ed.), *Second recent advances in quantitative remote sensing* (pp. 522–527). Spain: Publicacions de la Universitat de València.

Middleton, E. M., Corp, L. A., & Entcheva Campbell, P. K. (2007). Synthesis of leaf-level fluorescence, reflectance, and photosynthesis with linkage to canopy solar induced fluorescence. *Proceedings of the 3rd International Workshop on Remote Sensing of Vegetation Fluorescence, Florence, Italy, 7–9 February 2007*.

Middleton, E. M., Corp, L. A., & Entcheva Campbell, P. K. (2008). Comparison of measurements and FluorMOD simulations for solar-induced chlorophyll fluorescence and reflectance of a corn crop under nitrogen treatments. *International Journal of Remote Sensing*, *29*, 5193–5213.

Middleton, E. M., Corp, L., Entcheva Campbell, P. K., & Daughtry, C. (2006). Relating canopy hyperspectral reflectance and fluorescence indices to carbon related vegetation parameters. *Geoscience and Remote Sensing Symposium* (pp. 3760–3764). IGARSS 2006.

Miller, J. R., Berger, M., Goulas, Y., Jacquemoud, S., Louis, J., Mohammed, G., et al. (2005). Development of a vegetation fluorescence canopy model. *ESTEC Contract No. 1635/02/NL/FF, Final Report*.

Milton, E. J., Schaepman, M. E., Anderson, K., Kneubühler, M., & Fox, N. (2009). Progress in field spectroscopy. *Remote Sensing of Environment*, *113*, S92–S109.

Moya, I., Camenen, L., Evain, S., Goulas, Y., Cerovic, Z. G., Latouche, G., et al. (2004). A new instrument for passive remote sensing: 1. Measurements of sunlight-induced chlorophyll fluorescence. *Remote Sensing of Environment*, *91*, 186–197.

Moya, I., Camenen, L., Latouche, G., Mauxion, C., Evain, S., & Cerovic, Z. G. (1999). An instrument for the measurement of sunlight excited plant fluorescence. In G. Garab (Ed.), *Photosynthesis: Mechanisms and effects* (pp. 4265–4270). Dordrecht: Kluwer Academic Publishers.

Moya, I., Ounis, A., Moise, N., & Goulas, Y. (2006). First airborne multiwavelenght passive chlorophyll fluorescence measurements over La Mancha (Spain) fields. In J. A. Sobrino (Ed.), *Second recent advances in quantitative remote sensing* (pp. 820–825). Spain: Publicacions de la Universitat de València.

Olioso, A., Méthy, M., & Lacaze, B. (1992). Simulation of canopy fluorescence as a function of canopy structure and leaf fluorescence. *Remote Sensing of Environment*, *41*, 239–247.

Papageorgiou, G. C., & Govindjee (Eds.). (2004). *Chlorophyll a fluorescence: A signature of photosynthesisIn Advances in Photosynthesis and Respiration*, *Vol. 19*. Dordrecht: Kluwer Academic Publishers.

Pedrós, R., Jacquemoud, S., Goulas, Y., Louis, J., & Moya, I. (2005). A new leaf fluorescence model. *Proceedings of the 2nd Workshop on Remote Sensing of Solar Induced Vegetation Fluorescence, Montreal, Canada, 17–19 November 2004*.

Pérez-Priego, O., Zarco-Tejada, P. J., Miller, J. R., Sepulcre-Canto, G., & Fereres, E. (2005). Detection of water stress in orchard trees with a high-resolution spectrometer through chlorophyll fluorescence in-filling of the O_2-A band. *IEEE Transactions on Geoscience and Remote Sensing*, *43*, 2860–2869.

Plascyk, J. A. (1975). The MK II Fraunhofer line discriminator (FLD-II) for airborne and orbital remote sensing of solar-stimulated luminescence. *Optical Engineering*, *14*, 339–346.

Plascyk, J. A., & Gabriel, F. C. (1975). The Fraunhofer Line Discriminator MKII— An airborne instrument for precise and standardized ecological luminescence measurements. *IEEE Transaction on Instrumentation and Measurement*, *24*, 306–313.

Rosema, A., Snel, J. F. H., Zahn, H., Buurmeijer, W. F., & van Hove, L. W. A. (1998). The relation between laser induced chlorophyll fluorescence and photosynthesis. *Remote Sensing of Environment*, *65*, 143–154.

Sioris, C. E., Bazalgette Courrèges-Lacoste, G., & Stoll, M. P. (2003). Filling in of Fraunhofer lines by plant fluorescence: Simulations for a nadir-viewing satellite-borne instrument. *Journal of Geophysical Research*, *108*(D4), 3.1–3.6.

Stellmes, M., Schickling, A., Werner, W., & Hill, J. (2007). Detection of chlorophyll fluorescence by active and passive methods — Field experiments with barley. *Proceedings of the 3rd International Workshop on Remote Sensing of Vegetation Fluorescence, Florence, Italy, 7–9 February 2007*.

Theisen, A. F. (2002). Detecting chlorophyll fluorescence from orbit: The Fraunhofer Line Depth model. In R. S. Muttiah (Ed.), *From Laboratory Spectroscopy to Remotely Sensed Spectra of Terrestrial Ecosystems* (pp. 203–232). Dordrecht: Kluwer Academic Publishers1-4020-0753-1.

Ustin, S. L., Asner, G. P., Gamon, J. A., Jacquemoud, S., Ollinger, S., Schaepman, M., et al. (2006). Retrieval of quantitative and qualitative information about plant pigment systems from high resolution spectroscopy. *Proceedings of Geoscience and Remote Sensing Symposium, IGARSS, Denver, CO, USA, July 2006, 1996–1999*.

Van der Tol, C., Verhoef, W., & Rosema, A. (2009). A model for chlorophyll fluorescence and photosynthesis at leaf scale. *Agricultural and Forest Meteorology*, *149*(1), 96–105.

Verhoef, W. (1984). Light scattering by leaf layers with application to canopy reflectance modeling: The SAIL model. *Remote Sensing of Environment*, *16*, 125–141.

Verhoef, W. (2005). Extension of SAIL to model solar-induced canopy fluorescence spectra. *Proceedings of the 2nd Workshop on Remote Sensing of Vegetation Fluorescence, Montreal, Canada, 17–19 November 2004*.

Vila-Francés, J., Amorós-López, J., Alonso, L., Gómez-Chova, L., Calpe, J., del Valle-Tascón, S., et al. (2006). Vegetation fluorescence spectrum and Kautsky effect measurements under natural solar illumination. In J. A. Sobrino (Ed.), *Second recent advances in quantitative remote sensing* (pp. 985–990). Spain: Publicacions de la Universitat de València.

Zarco-Tejada, P. J., Berni, J. A. J., Suárez, L., Sepulcre-Cantó, G., Morales, F., & Miller, J. R. (2009). Imaging chlorophyll fluorescence with an airborne narrow-band multispectral camera for vegetation stress detection. *Remote Sensing of Environment*, *113*, 1262–1275.

Zarco-Tejada, P. J., Miller, J. R., Haboudane, D., Tremblay, N., & Apostol, S. (2003). Detection of chlorophyll fluorescence in vegetation from airborne hyperspectral CASI imagery in the red edge spectral region. *Geoscience and Remote Sensing Symposium* (pp. 598–600). IGARSS 2003.

Zarco-Tejada, P. J., Miller, J. R., Mohammed, G. H., & Noland, T. L. (2000). Chlorophyll fluorescence effects on vegetation apparent reflectance: I. Leaf-level measurements and model simulation. *Remote Sensing of Environment*, *74*, 582–595.

Zarco-Tejada, P. J., Miller, J. R., Mohammed, G. H., Noland, T. L., & Sampson, P. H. (2000). Chlorophyll fluorescence effects on vegetation apparent reflectance: II. Laboratory and airborne canopy-level measurements with hyperspectral data. *Remote Sensing of Environment*, *74*, 596–608.

Zarco-Tejada, P. J., Miller, J. R., Mohammed, G. H., Noland, T. L., & Sampson, P. H. (2001). Estimation of chlorophyll fluorescence under natural illumination from hyperspectral data. *International Journal of Applied Earth Observation and Geoinformation*, *3*, 321–327.

Zarco-Tejada, P. J., Miller, J. R., Pedrós, R., Verhoef, W., & Berger, M. (2006). FluorMODgui V3.0: A graphic user interface for the spectral simulation of leaf and canopy chlorophyll fluorescence. *Computers & Geosciences*, *32*, 577–591.

Zarco-Tejada, P. J., Pushnik, J. C., Dobrowski, S. Z., & Ustin, S. L. (2003). Steady state chlorophyll a fluorescence detection from canopy derivative reflectance and double-peak red-edge effects. *Remote Sensing of Environment*, *84*, 283–294.